Journal of Magnetic Resonance **155,** 83–91 (2002)
doi:10.1006/jmre.2002.2511, available online at http://www.idealibrary.com on IDEAL®

Efficiency of Homonuclear Hartmann–Hahn and COSY-Type Mixing Sequences in the Presence of Scalar and Residual Dipolar Couplings

Frank Kramer and Steffen J. Glaser[1]

Institut für Organische Chemie und Biochemie II, Technische Universität München, Lichtenbergstr. 4, D-85747 Garching, Germany

Received August 21, 2001; revised December 5, 2001

In the presence of scalar (J) and residual dipolar (D) couplings, the transfer efficiency of homonuclear Hartmann–Hahn and COSY-type mixing depends on the ratio D/J and on the mixing sequence. This dependence is analyzed theoretically and the results are confirmed experimentally. At least two different mixing sequences are required to yield good transfer efficiencies for all ratios D/J. In contrast to COSY-type experiments, homonuclear Hartmann–Hahn sequences can provide efficient transfer even if the sum of D and J is zero, i.e., if the coupling vanishes in the weak coupling limit.

Key Words: **Hartmann–Hahn transfer; residual dipolar couplings; dipolar mixing; TOCSY; DCOSY; COSY.**

INTRODUCTION

Residual dipolar couplings yield valuable structural information in high-resolution NMR (*1–5*). Homonuclear Hartmann–Hahn (TOCSY) transfer (*6–8*) through residual dipolar couplings (dipolar mixing) and through J couplings (isotropic mixing) have many common features (*4, 8, 9*). However, the specific forms of isotropic and dipolar coupling tensors give rise to very different transfer dynamics (*4, 8, 10, 11*). In addition, the distinct transformation properties under rotations can result in very different scaling properties of isotropic and dipolar coupling tensors under the same multiple pulse sequence (*9, 12*). This also leads to a distinct offset dependence of the transfer efficiency (*9*). Modified phase-cycled Carr–Purcell-type (MOCCA) multiple-pulse sequences have been developed (*13*) that make it possible to achieve considerably improved dipolar scaling factors compared to DIPSI-2 (*14*), MLEV-16 (*15*), or MLEV-17 (*7*). Here we present a systematic study of the transfer efficiency of important experimental building blocks if scalar (J) and residual dipolar (D) couplings are superimposed. For commonly used mixing sequences, dramatic differences are found in the transfer efficiency as a function of D/J. This perhaps surprising behavior can be rationalized and simple rules will be presented to predict the transfer efficiency of a given pulse-sequence element. In practice, these rules make it possible to choose the most suitable pulse sequences for a given application.

THEORY

We consider a system of two coupled homonuclear spins 1/2 with the free evolution Hamiltonian

$$\mathcal{H}_0 = \mathcal{H}_{off} + \mathcal{H}_J + \mathcal{H}_D \qquad [1]$$

with the offset term

$$\mathcal{H}_{off} = 2\pi\nu_1 I_{1z} + 2\pi\nu_2 I_{2z}, \qquad [2]$$

the scalar coupling term

$$\mathcal{H}_J = 2\pi J(I_{1z}I_{2z} + I_{1x}I_{2x} + I_{1y}I_{2y}), \qquad [3]$$

and the residual dipolar coupling term

$$\mathcal{H}_D = 2\pi D\left(I_{1z}I_{2z} - \frac{1}{2}I_{1x}I_{2x} - \frac{1}{2}I_{1y}I_{2y}\right). \qquad [4]$$

Here, the residual dipolar coupling constant is given by

$$D_{kl} = -S\frac{\mu_0\gamma^2\mathrm{h}}{8\pi^2 r_{kl}^3}\left\{A_a(3\cos^2\theta - 1) + \frac{3}{2}A_r(\sin^2\theta\cos 2\phi)\right\}, \qquad [5]$$

where S is a generalized order parameter, γ is the gyromagnetic ratio, r_{kl} is the internuclear distance, and A_a and A_r are the axial and rhombic components of the molecular alignment tensor, in whose principal axis system the bond vector is defined by the cylindrical coordinates θ and ϕ. This definition of $\mathcal{H}_D$ is consistent with the most widely used convention (see, e.g., (*16, 17*)) but differs (in magnitude and/or sign) from the definition of the residual dipolar coupling constant in other texts (see, e.g., (*9, 11, 13, 18*)). During a multiple pulse sequence with radio frequency (rf) amplitude $\nu_{rf}(t)$ and phase $\varphi(t)$, the Hamiltonian

[1] To whom correspondence should be addressed.

1090-7807/02 $35.00

is given by $\mathcal{H}_0 + \mathcal{H}_{rf}(t)$ with the rf term

$$\mathcal{H}_{rf}(t) = 2\pi\nu_{rf}(t)\{(I_{1x} + I_{2x})\cos\varphi(t) + (I_{1y} + I_{2y})\sin\varphi(t)\}. \quad [6]$$

The evolution of the density operator is governed by the Liouville–von Neuman equation (*19*), which can always be solved numerically, using NMR simulation programs such as SIMONE (*20*).

However, in order to better understand the properties of dipolar mixing experiments, an analysis based on average Hamiltonian theory (*8, 19, 21*) is very helpful. In the effective Hamiltonian created by Hartmann–Hahn-type mixing sequences, the offset term $\mathcal{H}_{off}$ must be suppressed and the transfer of coherence and polarization is governed by the form of the effective coupling term (*8*)

$$\mathcal{H}_C^{eff} = \mathcal{H}_J^{eff} + \mathcal{H}_D^{eff} = 2\pi\,\mathbf{I_1}\mathbf{C}^{eff}\mathbf{I_2}. \quad [7]$$

In the toggling frame defined by the action of $\mathcal{H}_{off} + \mathcal{H}_{rf}(t)$, the elements $\bar{C}^{ij}_{\alpha\beta}$ of the zero-order term $\bar{\mathbf{C}}$ of the effective coupling tensor $\mathbf{C}^{eff}$ are given by (*8, 9*)

$$\bar{C}^{ij}_{\alpha\beta} = \frac{1}{\tau_c}\int_0^{\tau_c}\left((J + D)a^i_{z\alpha}(t)a^j_{z\beta}(t) + \left(J - \frac{D}{2}\right)a^i_{x\alpha}(t)a^j_{x\beta}(t) + \left(J - \frac{D}{2}\right)a^i_{y\alpha}(t)a^j_{y\beta}(t)\right)dt, \quad [8]$$

where $\alpha, \beta = x,\ y$, or z and τ_c is the cycle time of the multiple pulse sequence. The coefficients $a^i_{\alpha\beta}$ and $a^j_{\alpha\beta}$ are the elements of a real, three-dimensional rotation matrix, which transforms the spin operators $I_{i\alpha}$ and $I_{j\beta}$ in the toggling frame (*8, 9*). For offsets that are small compared to the rf field, the analysis can be considerably simplified. In this limit, all rotations are nonselective, leaving the isotropic coupling term $\mathcal{H}_J$ invariant (*8*); i.e., $\bar{\mathcal{H}}_J = \mathcal{H}_J$, and only the form of the dipolar coupling term is modified in the average Hamiltonian.

In many cases of practical interest, the form of the dipolar coupling tensor is conserved in the average Hamiltonian, except for a scaled average dipolar coupling constant $\bar{D}$ and a relabeling of the coordinate axes:

$$\bar{\mathcal{H}}_D = 2\pi\bar{D}\left(I_{1z'}I_{2z'} - \frac{1}{2}I_{1x'}I_{2x'} - \frac{1}{2}I_{1y'}I_{2y'}\right). \quad [9]$$

For example, for DIPSI-2 (*14*), $\bar{\mathcal{H}}_D = 2\pi D(-1/2I_{1x}I_{2x} + 1/4I_{1y}I_{2y} + 1/4I_{1z}I_{2z})$ (*12*) which can be expressed in the form of Eq. [9] with $\bar{D} = -\mathrm{D}/2$ and the principal axis $z' = x$. In Table 1, the dipolar scaling factors

$$s_D = \bar{D}/D \quad [10]$$

and the principal axes z' are summarized for the mixing sequences DIPSI-2 (*14*), MOCCA-XY16 (*13*), Clean MLEV-17 (*22*), MLEV-16 (*15*), and MLEV-17 (*7*). In the limit of hard pulses, the MOCCA-M16 sequence (*13*) also creates an average dipolar coupling tensor of the form of Eq. [9] with the same dipolar scaling factor $s_D = 1$ and the same principal axis system as the MOCCA-XY16 sequence. Note that the dipolar scaling factor of the MOCCA sequences is up to a factor of 4 larger compared to commonly used TOCSY mixing sequences, such as MLEV-17, resulting in a corresponding increase of the transfer rates for purely dipolar coupled spins. It is also interesting to note that for Clean MLEV-17 the dipolar scaling factor is a factor of 2 larger than for MLEV-17.

TABLE 1

Maximum On-Resonance Dipolar Scaling Factors s_D, "Blind Spots" $(D/J)^0_{P,L}$, and Principal Axis z' of the Effective Dipolar Coupling Tensor for Characteristic Hartmann–Hahn-Type Mixing Sequences

Sequence	s_D	$(D/J)^0_P$	$(D/J)^0_L$	z'
DIPSI-2	−0.5	−4	2	x
MOCCA-XY16, MOCCA-M16	1	2	−1	z
Clean MLEV-17	0.5	4	−2	y
MLEV-16, MLEV-17	0.25	8	−4	y

Note. The following mixing sequences (and standard phases) are assumed: DIPSI-2 (with phases $x, -x, -x, x$) (*14*), MOCCA-XY16 (*9*), MOCCA-M16 (*9*), Clean MLEV-17 (*22*), MLEV-16 (*15*), and MLEV-17 (where the composite 180° pulse is given by $90°_x, 180°_y, 90°_x$ and the "17th" pulse is $60°_y$) (*7*).

If both isotropic and dipolar couplings are present, the zero-order effective coupling term has the form

$$\bar{\mathcal{H}}_C = \bar{\mathcal{H}}_J + \bar{\mathcal{H}}_D = 2\pi\{C^L I_{1z'}I_{2z'} + C^P(I_{1x'}I_{2x'} + I_{1y'}I_{2y'})\} \quad [11]$$

with the effective longitudinal and planar coupling constants

$$C^L = J + \bar{D} = J + s_D \cdot D \quad [12]$$

and

$$C^P = J - \frac{1}{2}\bar{D} = J - s_D \cdot D/2. \quad [13]$$

If $\bar{\mathcal{H}}_C$ has the form of Eq. [11], it is called a cylindrical mixing Hamiltonian (*18, 23*) in the principal axis system (x', y', z') of the effective coupling tensor, where all polarization transfer

functions are defined (*8*) as

$$T_{\alpha'} = \frac{Tr\{e^{-i\bar{\mathcal{H}}_C\tau} I_{1\alpha'} e^{i\bar{\mathcal{H}}_C\tau} I_{2\alpha'}\}}{Tr\{I_{2\alpha'} I_{2\alpha'}\}}.$$

For two coupled spins, longitudinal and transverse transfer functions $T_{z'}$ and $T_{x'} = T_{y'}$ under cylindrical mixing conditions are given by (*8, 18, 23*)

$$T_{z'} = \sin^2(\pi C^P \tau) \quad [14]$$

and

$$T_{x'} = T_{y'} = \sin(\pi C^P \tau)\sin(\pi C^L \tau). \quad [15]$$

Note that both the longitudinal and transverse transfer functions vanish for $C^P = 0$, which is the case if the ratio of residual dipolar and scalar coupling constants is given by

$$(D/J)_P^0 = 2/s_D. \quad [16]$$

The transverse transfer functions also vanish for $C^P = 0$ (i.e., for $(D/J)_P^0 = 2/s_D$) and in addition for $C^L = 0$, which is found for

$$(D/J)_L^0 = -1/s_D. \quad [17]$$

The values of $(D/J)_P^0$ and $(D/J)_L^0$ are summarized in Table 1 for DIPSI-2, MOCCA-XY16, MOCCA-M16, Clean MLEV-17, MLEV-16, and MLEV-17.

The transfer efficiency depends on the transfer amplitude as well as on the transfer time. In practice, transfer functions are dampened by relaxation. Here, we use the following definition of the transfer efficiency η:

$$\eta_\alpha = \max_{\tau>0}\{|T_\alpha(\tau)|\exp(-\tau/\tau_{damp})\}. \quad [18]$$

In the following calculations, the time constant τ_{damp} of the exponential damping factor is chosen to be

$$\tau_{damp} = 1/|J| \quad [19]$$

for simplicity (*8, 24*). However, in practical applications the situation is more complicated and effective relaxation rates (*8*) must be taken into account for a detailed comparison of pulse sequences. Fig. 1 shows the dampened longitudinal and transverse transfer functions $T_{z'}$ and $T_{x'}$ as a function for D/J for characteristic mixing sequences listed in Table 1.

For comparison, we also consider transfer functions for a COSY-type mixing step based on pulse-interrupted delays. These experiments can in general be described in the weak coupling limit, where the coupling term $\mathcal{H}_C = \mathcal{H}_J + \mathcal{H}_D$ simplifies to

$$\mathcal{H}_C^{\text{weak}} = 2\pi(J + D)I_{1z}I_{2z}. \quad [20]$$

Hence, for such experiments the coupling vanishes completely for $J + D = 0$, which corresponds to the ratio

$$(D/J)_L^{0,\,\text{COSY}} = -1 \quad [21]$$

where no COSY-type transfer is possible.

Although in COSY experiments the actual transfer mechanism is antiphase to antiphase, the excited magnetization is inphase and also only inphase magnetization is directly observable. Hence, for comparison, we consider the sequence $(\tau/4) - (\pi)_x - (\tau/4) - (\pi/2)_x - (\tau/4) - (\pi)_x - (\tau/4)$ (representing a homonuclear version of refocused INEPT transfer (*25*)) as a representative of in-phase transfer based on pulse-interrupted free precession sequences, which has the following overall transfer function for x magnetization

$$T_x^{COSY} = \sin^2(\pi(J + D)\tau/2). \quad [22]$$

The transfer efficiency of longitudinal (z') Hartmann–Hahn transfer and transverse (x) COSY-type transfer is shown in Fig. 2A, and the transfer efficiency of transverse (x') Hartmann–Hahn transfer is shown in Fig. 2B. As expected, for $D/J = 0$ all Hartmann–Hahn-type experiments have identical transfer functions and hence identical transfer efficiencies η, which correspond to the case of isotropic mixing. However, for $D/J \neq 0$, the different mixing sequences have markedly different transfer efficiencies. Each sequence has at least one "blind spot" and none of these experiments can yield efficient transfer for all ratios of D/J. The minima of the transfer efficiencies η as a function of D/J are given by Eqs. [16], [17], and [21]. A minimum of two experiments (e.g., a longitudinal MOCCA-type and a COSY-type experiment) are required to yield efficient polarization transfer for all possible ratios of D/J. As transverse Hartmann–Hahn-type transfer has not only one but two "blind spots" (see Fig. 2B and Eqs. [16], [17]), the transfer of x' or y' coherence is unfavorable if the relative size of D and J varies in a given application, such as in H_N–H_α correlations in peptides and proteins (*26*).

EXPERIMENTAL

In order to test the theoretical predictions, experimental coherence and polarization transfer functions between H5 and H6 of cytosine were acquired in isotropic and anisotropic solutions. Four samples were prepared with phage (PF1-LP11-92, ASLA Ltd., Latvia) concentrations between 0 and 50 mg/ml. The various sample conditions (pH) and the residual quadrupolar splitting of the D_2O signal are summarized in Table 2. In addition, the experimentally determined isotropic (J) and dipolar (D)

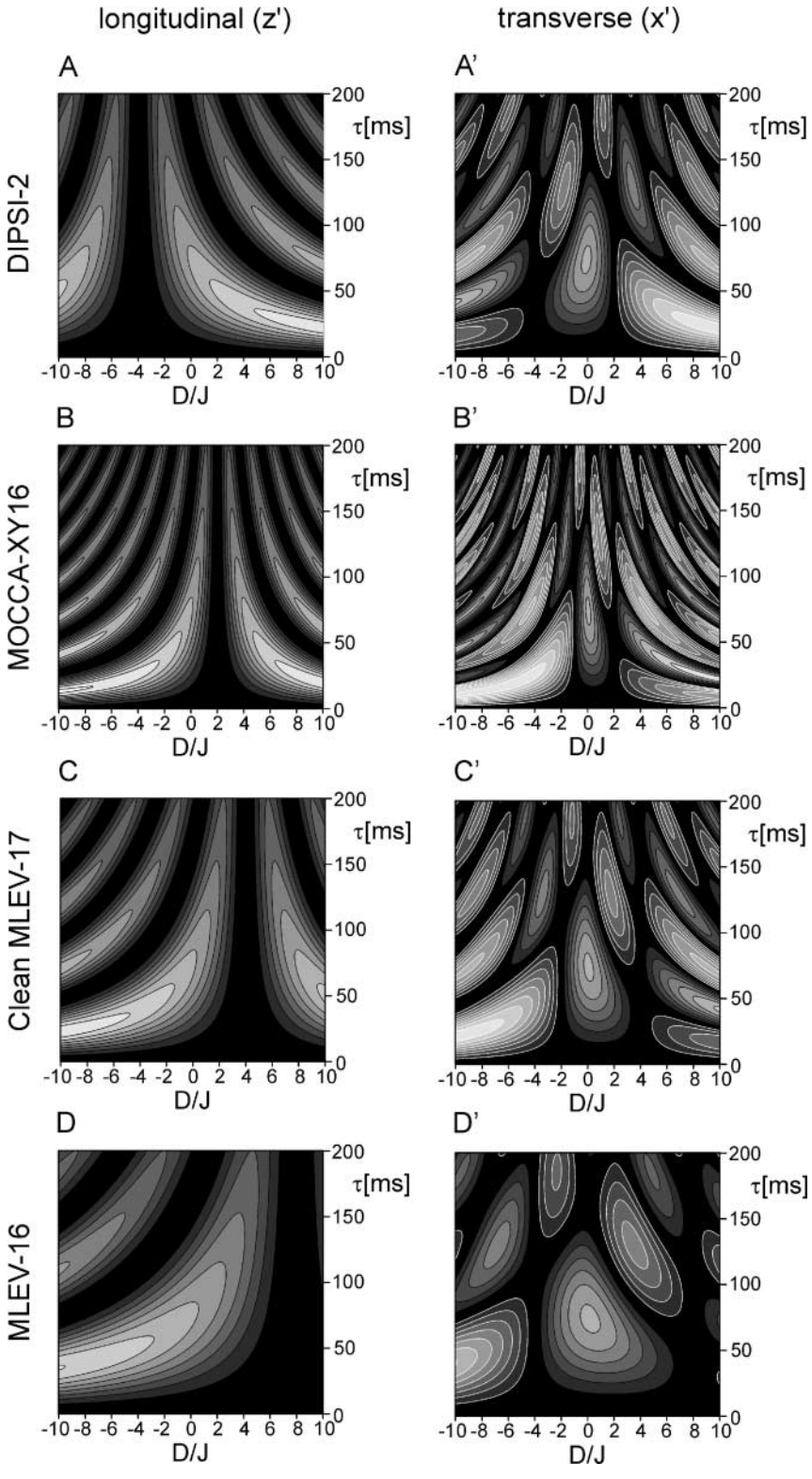

FIG. 1. Dampened longitudinal (A–D) and transverse (A′–D′) transfer functions $T_{z'}$ and $T_{x'}$ as a function of D/J for the Hartmann–Hahn-type mixing sequences DIPSI-2 (A, A′), MOCCA-XY16 (B, B′), Clean MLEV-17 (C, C′), MLEV-16 (D, D′) (see Table 1). The transfer functions were simulated using the program SIMONE (*20*) where the effects of rf inhomogeneity were considered by assuming a Gaussian rf inhomogeneity distribution with a full width of 10% at half height. A scalar coupling constant of $J = 6$ Hz was assumed in the simulations. The simulated transfer functions were multiplied by the damping function $e^{-\tau/\tau_{damp}}$ with $\tau_{damp} = 1/J = 166$ ms (cf. Eq. [19]). Black and white lines represent positive and negative contours, respectively. Contour lines are shown for ± 0.1, $\pm 0.2, \ldots, \pm 0.9$. Areas with the same absolute value of the transfer amplitudes $T_{\alpha'}$ are filled by the same gray level (e.g., black for $|T_{\alpha'}| \leq 0.1$).

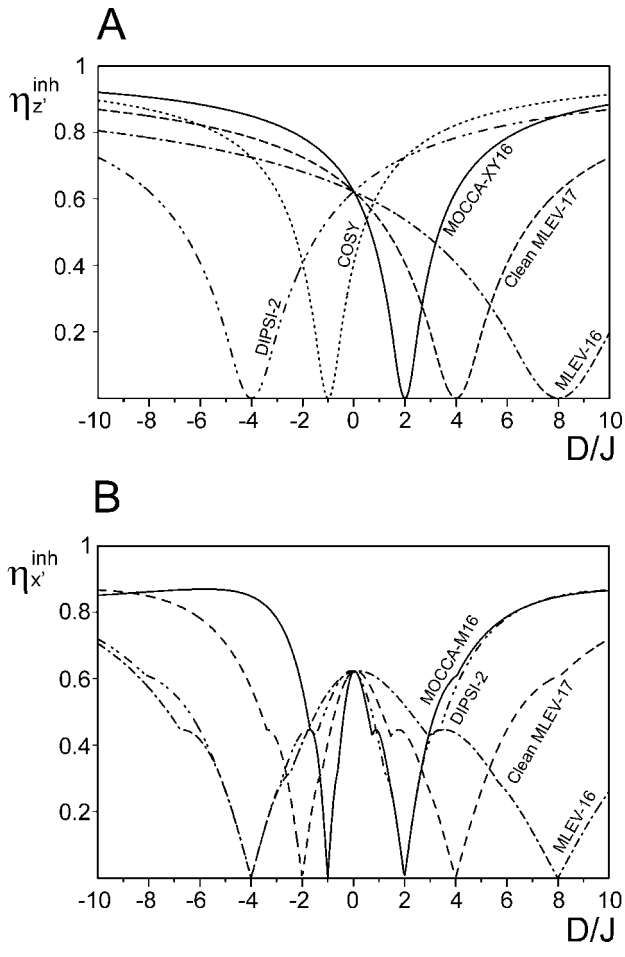

FIG. 2. Transfer efficiency $\eta_{\alpha'}^{inh}$ (cf. Eq. [18]) of (A) polarization (z') and (B) coherence (x') transfer under the following Hartmann–Hahn-type mixing sequences: DIPSI-2 (– – –), MOCCA-XY16 (—), Clean MLEV-17 (– –), and MLEV-16 (– – – –) (see Table 1). The transfer efficiency $\eta_{\alpha'}^{inh}$ (Eq. [18]) was determined based on the simulated transfer functions shown in Fig. 1. In addition, the theoretical transfer efficiency of COSY-type experiments (- -) is shown in (A) based on the analytical transfer function T_x^{COSY} given in Eq. [22].

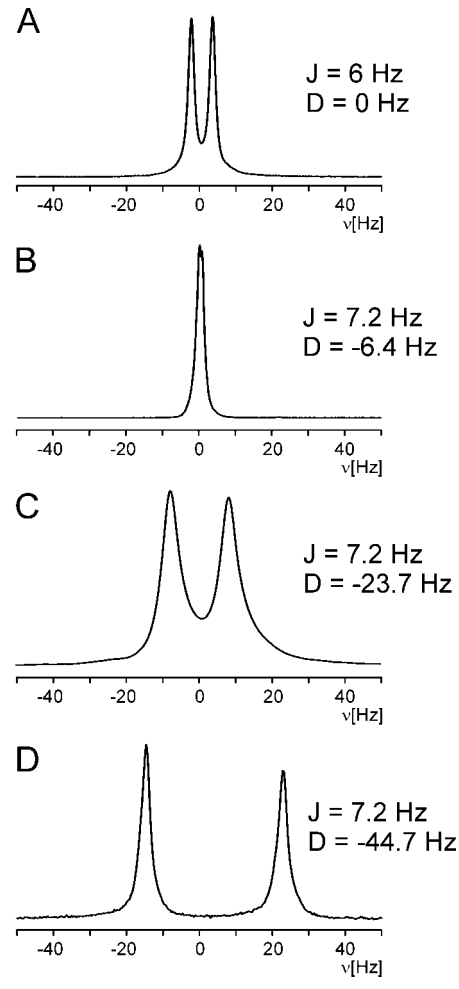

FIG. 3. H6 resonance of cytosine in the four sample preparations (see Table 2) with doublet splittings of (A) $J + D = 6$ Hz, (B) $J + D = 0.8$ Hz (unresolved), (C) $J + D = -16.5$ Hz, and (D) $J + D = -37.5$ Hz.

coupling constants, the observed splittings of the doublets ($J + D$) and the ratios D/J are summarized in Table 2. The experimentally observed doublet of the H6 resonance with splitting $J + D$ is shown in Fig. 3 for the four samples.

TABLE 2
Experimental Parameters of the Prepared Samples of Cytosine

Sample	Phage conc. [mg/ml]	pH	$Q(D_2O)$ [Hz]	J [Hz]	D [Hz]	$J + D$ [Hz]	D/J [Hz]
1	–	14	0	6.0	0	6.0	0
2	~5	6.5	7.9	7.2	−6.4	0.8	−0.89
3	~20	7	30.4	7.2	−23.7	−16.5	−3.29
4	~45	7.5	60.1	7.2	−44.7	−37.5	−6.21

Note. In samples 2–4, J was measured in isotropic solution at the corresponding pH.

In Figs. 4 and 5, experimental longitudinal and transverse transfer functions between H5 and H6 are shown for DIPSI-2 (*14*), MOCCA-XY16 (*13*), MOCCA-M16 (*13*), Clean MLEV-17 (*22*), MLEV-16 (*15*), and MLEV-17 (*7*). In the preparation period of these experiments, the H6 resonance was selectively saturated using CW irradiation and a series of one-dimensional experiments with Hartmann–Hahn mixing periods τ between 0 and 200 ms was acquired (*10*). In Figs. 4 and 5, the experimental transfer functions are represented by black dots, which correspond to the integrated intensity of the H6 signal as a function of the mixing time τ.

For comparison, simulated transfer functions are also shown in Figs. 4 and 5 (solid lines). These simulations were made using an extended version of the program SIMONE (*20*). In the simulations, the experimentally determined coupling constants, offsets ($\upsilon_1 = 460$ Hz and $\upsilon_2 = -460$ Hz for the anisotropic samples near pH 7, $\upsilon_1 = 560$ Hz and $\upsilon_2 = -560$ Hz for the isotropic sample at pH 14), and the parameters (see Table 3) of the experimental

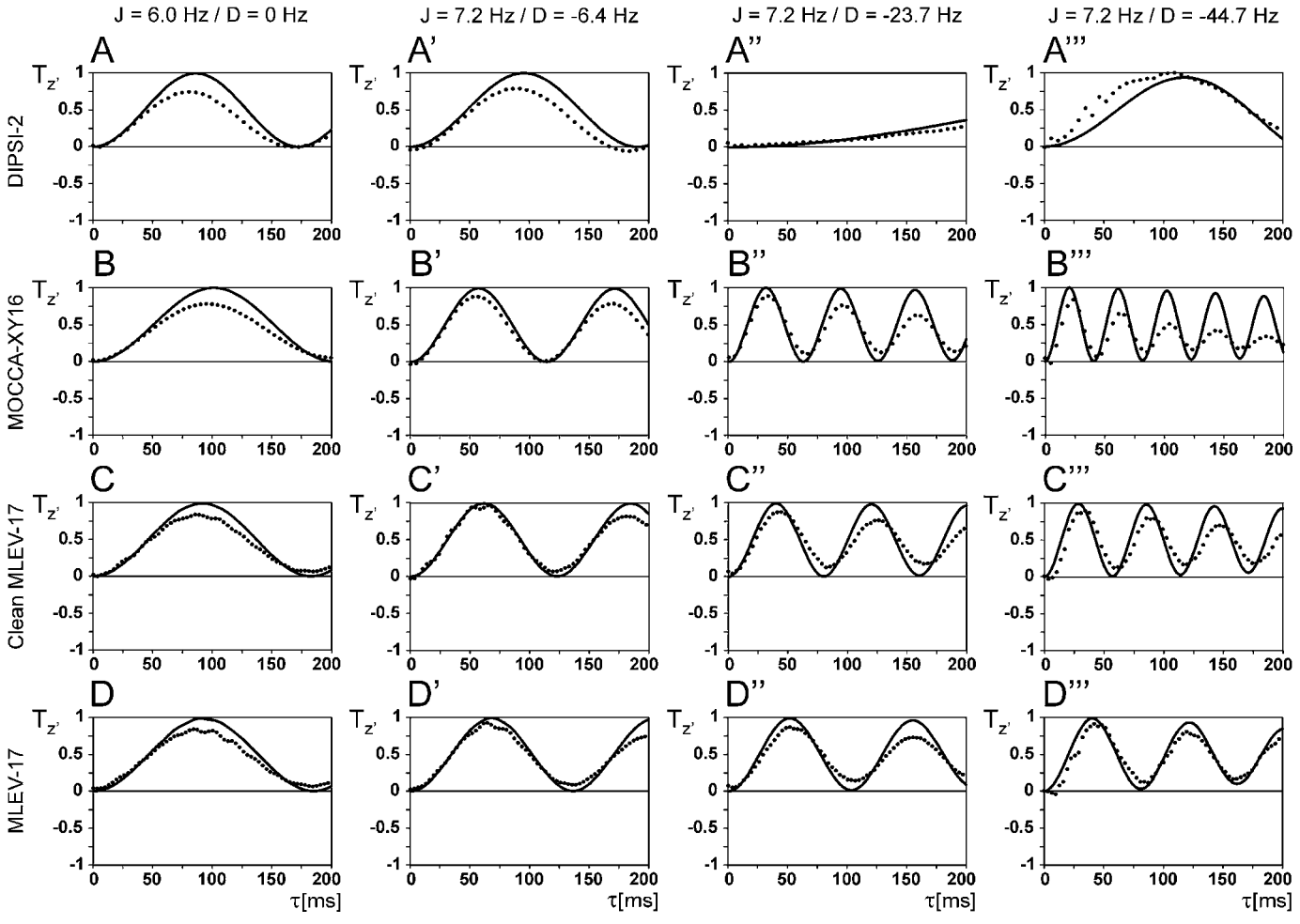

FIG. 4. Simulated (—) and experimental (●) longitudinal transfer functions $T_{z'}$ for DIPSI-2 (A–A‴), MOCCA-XY16, (B–B‴), Clean MLEV-17 (C–C‴), and MLEV-17 (D–D‴) for z' transfer between H5 and H6 of cytosine (see text and Table 3 for experimental details). Panels (A–D), (A′–D′), (A″– D″), and (A‴–D‴) correspond to the values of J and D in Samples 1, 2, 3, and 4, respectively (see Table 2).

mixing sequences with approximately identical rf power (corresponding to root mean square rf amplitude $\nu_{rf}^{rms} \approx 5$ kHz) were taken into account. In addition, the effects of rf inhomogeneity were considered, assuming a Gaussian rf inhomogeneity distribution with a full width of 10% at half height (*8*). A reasonable match is found between experimental and simulated transfer functions. The remaining discrepancies are mainly attributed to inhomogeneous distribution of residual dipolar couplings in the sample.

TABLE 3
Experimental Pulse Sequence Parameters

Sequence	ν_{rf} [kHz]	$\tau_{180°}$ [μs]	Δ [μs]	ν_{rf}^{rms} [kHz]
DIPSI-2	5	100	—	5
MOCCA-XY16, MOCCA-M16	15.2	33	264	5.1
Clean MLEV-17	7.1	70.71	35.36	5.8
MLEV-16, MLEV-17	5	100	—	5

The experimental and simulated transfer functions also match well with the results of our simplified theoretical analysis in the previous section, which assumed that both spins are on-resonance. As expected, all curves are approximately identical for sample 1 (Figs. 4A–4D and 5A–5C), where $D = 0$ and $T_{x'} = T_{y'} = T_{z'}$ (cf. Eqs. [14] and [15]) with $C^P = C^L = J$. Here, the optimal transfer is found near $1/(2J) \approx 80$ ms. However, for oriented samples with $D \neq 0$, the transfer functions depend strongly on the size of the residual dipolar coupling constant D, the mixing sequence and the type of transfer (longitudinal or transverse).

As expected (cf. Eq. [14]), in Fig. 4, the simulated and experimental longitudinal transfer functions $T_{z'}$ are all positive and the first maximum is found near $|1/(2C^P)| = |1/(2J - s_D D)|$ (cf. Eq. [13]). Based on Figs. 1A–1D and Fig. 2A, the most efficient polarization transfer for the oriented samples of cytosine

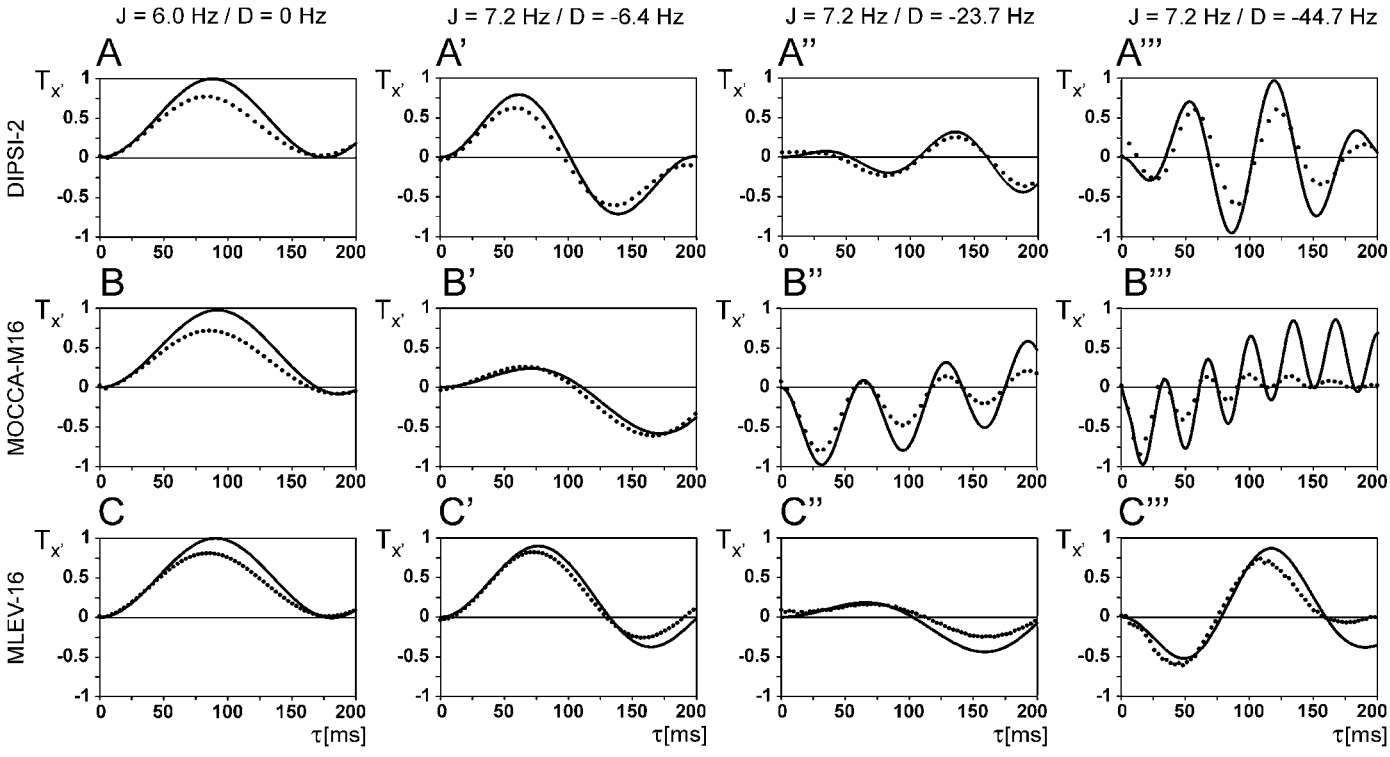

FIG. 5. Simulated (—) and experimental (●) transverse transfer functions $T_{x'}$ for DIPSI-2 (A–A‴), MOCCA-M16 (B–B‴), and MLEV-16 (C–C‴) for x' transfer between H5 and H6 of cytosine (see text Table 3 for experimental details). Panels (A–C), (A′–C′), (A″–C″) and (A‴–C‴) correspond to the values of J and D in Samples 1, 2, 3, and 4, respectively (see Table 2).

with $D/J < 0$ is expected for the MOCCA-XY16 sequence (Figs. 4B′–4B‴), followed by Clean MLEV-17 (Figs. 4C′–4C‴), MLEV-17 (Figs. 4D′–4D‴), and DIPSI-2 (Figs. 4A′–4A‴). In fact, the fastest longitudinal transfer is found in Fig. 4B‴ for the MOCCA-XY16 sequence, where with $J = 7.2$ Hz, $D = -44.7$ Hz (cf. Table 2, sample 4) and an ideal scaling factor $s_D = 1$ (cf. Table 1) the first maximum would be expected at a mixing time $\tau = |1/(2C^P)| = 17$ ms. For a realistic scaling factor (*13*) of $s_D \approx 0.8$, which corresponds to the experimental offsets and pulse sequence parameters (cf. Table 3), complete transfer is expected at $\tau = |1/(2C^P)| \approx 20$ ms, which closely matches the results of the simulated and experimental transfer functions in Fig. 4B‴. Note that in the same sample (sample 4), the transfer time is more than six times longer for the DIPSI-2 sequence with $s_D \approx -0.5$ (cf. Table 1), where the first maximum is found near $|1/(2C^P)| = 125$ ms (cf. Fig. 4A‴). In Fig. 4, the most inefficient polarization transfer is effected by DIPSI-2 in sample 3, where with $J = 7.2$ Hz, $D = -23.7$ Hz (cf. Table 2), and $s_D = -0.5$ the first maximum of the transfer function is expected only for a mixing time $\tau = |1/(2C^P)| \approx 400$ ms. Again, this is in full agreement with the theoretical predictions of Figs. 1A–1D and 2, because in sample 3 the ratio $D/J = -3.29$ is close to the "blind spot" for polarization transfer of DIPSI-2 at $(D/J)^0_P = -4$ (cf. Table 1).

For the case of transverse transfer (Fig. 5), the transfer functions $T_{x'}$ (cf. Eq. [15]) can be positive or negative. In addition to the "blind spots" of the sequences at $(D/J)^0_P$, the transverse transfer also vanishes at $(D/J)^0_L$. For example, in sample 3 the ratio $D/J = -3.29$ is close not only to $(D/J)^0_{P,\text{DIPSI-2}} = -4$ but also to $(D/J)^0_{L,\text{MLEV-16}} = -4$, resulting in poor transfer efficiency in Figs. 5A″ and 5C″. Conversely, in sample 2 the ratio $D/J = -0.89$ is close to $(D/J)^0_{L,\text{MOCCA-}M16} = -1$, resulting in poor transfer efficiency in Fig. 5B′. Again, as expected from the results of Figs. 1A′–1D′ and Fig. 2B, the most efficient transfer is found in sample 4 for the MOCCA-M16 sequence, where almost complete transfer (with inverted sign) is found for a mixing time of only 15 ms (cf. Fig. 5*B*‴).

In order to demonstrate the complementary transfer properties of COSY- and TOCSY-type experiments (see Fig. 2A), two-dimensional spectra were acquired for sample 2, where $D \approx -J$ (see Table 2). The splitting $J + D = 0.8$ Hertz is smaller than the line width and results in DQF-COSY cross peaks with low amplitudes because of mutual cancellation of the antiphase components of the cross-peak multiplet (see Fig. 6A). However, even if the doublet splitting is unresolved, efficient polarization transfer is possible in MOCCA-type experiments, where the full average coupling term $\bar{\mathcal{H}}_C$ (Eq. [11]) is active. In Fig. 6B, the corresponding cross peak is shown in a Hartmann–Hahn-type

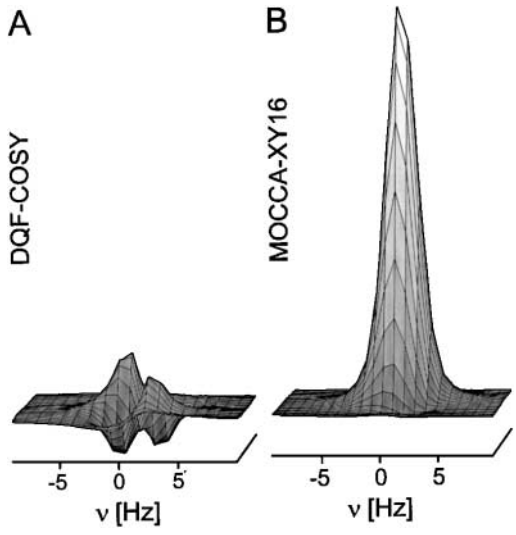

FIG. 6. Comparison of H5-H6 cross peak intensities in two-dimensional DQF-COSY (A) and MOCCA-XY16 (B) spectra of cytosine (sample 2, see Table 2) with $J = 7.2$ Hz and $D = -6.4$ Hz, where the doublet splitting $J + D = 0.8$ Hz is not resolved in the inphase multiplet (see Fig. 3B). The mixing time of the MOCCA-XY16 sequence was $\tau = 55$ ms.

experiment with a MOCCA-XY16 mixing sequence, where optimal polarization transfer ($T_{z'} = T_z$) is found for a mixing period τ of 55 ms (cf. Fig. 4B′). As expected from Fig. 2A, a large gain in cross-peak amplitude is found for the MOCCA-XY16 experiment compared to the COSY-type experiments for $D/J \approx (D/J)^0_{L,COSY} = -1$ (cf. Eq. [21]) where $\mathcal{H}_C^{weak} = 0$ (Eq. [20]). Conversely, COSY-type experiments would have significantly more intense cross peaks compared to MOCCA-type experiments for $D/J \approx (D/J)^0_{P,MOCCA} = 2/s_D \approx 2$ (cf. Eq. [13]), where the effective planar coupling constant C^P (cf. Eq. [13]) vanishes. However, with the prepared cytosine samples only positive D/J ratios were experimentally accessible (cf. Table 1).

CONCLUSION

The theoretical results derived in this paper form the basis for a rational choice of the mixing sequences in two-dimensional correlation experiments of spins that are connected through both scalar and residual dipolar couplings. In all experiments, the transfer efficiency is zero for at least one ratio D/J. In Hartmann–Hahn-type experiments, only one such "blind spot" is found for the transfer of polarization (z' magnetization; see Table 1), whereas for the transfer of coherence (x' and y' magnetization) two such "blind spots" exist. Hence, in this respect, the transfer of polarization is preferable to the transfer of coherence. The position of the "blind spots" (i.e., the ratio D/J for which the efficiency of polarization transfer is zero) depends on the dipolar scaling factor s_D (cf. Eqs. [16] and [17]) and hence on the dipolar mixing sequence (see Table 1).

In experiments where the relative size of D and J varies, such as in $H_N - H_\alpha$ correlations (31), two complementary experiments should be acquired in order to yield efficient transfer for all possible ratios D/J (see Fig. 2A). A MOCCA-type Hartmann–Hahn experiment and a COSY-type experiment form an almost ideal combination with complementary "blind spots" and favorable transfer characteristics (see Fig. 2). It is also important to note that coherence and polarization transfer functions are sensitive to the relative sign of J and D (see, e.g., Fig. 1), which may form the basis of a new approach to determine the sign of residual dipolar coupling constants. For homonuclear coupling networks consisting of more than two spins, the transfer functions are more complicated. However, for the case of three coupled spins 1/2, analytical longitudinal and transverse transfer functions are known for cylindrical mixing conditions (*18*). These analytical transfer functions are directly applicable if the principal axis z' (see Table 1) of the effective coupling tensor and the effective longitudinal and planar coupling constants $C^L = J + s_D D$ and $C^P = J - s_D D/2$ (Eqs. [12], [13]) are taken into account for a given multiple-pulse sequence. However, even for complicated coupling networks, the simple and efficient transfer dynamics of isolated two-spin systems can often be recovered in tailored correlation spectroscopy (TACSY) by using selective Hartmann–Hahn-type experiments (*8, 27*).

ACKNOWLEDGMENTS

SJG thanks the Fonds der Chemischen Industrie and the DFG for support (Gl 203/1-6 and 3-1). FK acknowledges a stipend from the Fonds der Chemischen Industrie. We thank Ad Bax for pointing out the cytosine model system.

REFERENCES

1. N. Tjandra and A. Bax, Direct measurement of distances and angles in biomolecules by NMR in a dilute liquid crystalline medium, *Science* **278,** 1111–1114 (1997).
2. A. Bax and N. Tjandra, High resolution NMR of human ubiquitin in an aqueous liquid crystalline medium, *J. Biomol. NMR* **10,** 289–292 (1997).
3. J. H. Prestegard, New techniques in structural NMR—Anisotropic interactions, in "NMR Supplement," *Nat. Struct. Biol.*, 517–522 (July, 1998).
4. M. R. Hansen, M. Rance, and A. Pardi, Observation of long-range ^{1}H–^{1}H distances in solution by dipolar coupling interactions, *J. Am. Chem. Soc.* **120,** 11,210–11,211 (1998).
5. M. R. Hansen, P. Hanson, and A. Pardi, Filamentous bacteriophage for aligning RNA, DNA, and proteins for measurement of nuclear magnetic resonance dipolar coupling interactions, *Methods Enzymol.* **317,** 220–240 (2000).
6. L. Braunschweiler and R. R. Ernst, Coherence transfer by isotropic mixing: Application to proton correlation spectroscopy, *J. Magn. Reson.* **53,** 521–528 (1983).
7. A. Bax and D. G. Davis, MLEV-17-based two-dimensional homonuclear magnetization transfer spectroscopy, *J. Magn. Reson.* **65,** 355–360 (1985).

8. S. J. Glaser and J. J. Quant, Homonuclear and heteronuclear Hartmann–Hahn transfer in isotropic liquids, *in* "Advances in Magnetic and Optical Resonance" (W. S. Warren, Ed.), Vol. 19, pp. 59–252, Academic Press, San Diego (1996).
9. F. Kramer, B. Luy, and S. J. Glaser, Offset dependence of homonuclear Hartmann–Hahn transfer based on residual dipolar couplings in solution state NMR, *Appl. Magn. Reson.* **17,** 173–187 (1999).
10. O. Schedletzky and S. J. Glaser, Analytical coherence transfer functions for the general AMX system under isotropic mixing, *J. Magn. Reson. A* **123,** 174–180 (1996).
11. B. Luy and S. J. Glaser, Analytical polarization and coherence transfer functions for three dipolar coupled spins 1/2, *J. Magn. Reson.* **142,** 280–287 (2000).
12. B. H. Meier, Polarization transfer and spin diffusion in solid-state NMR, *in* "Advances in Magnetic and Optical Resonance" (W. S. Warren, Ed.), Vol. 18, pp. 1–116, Academic Press, San Diego (1994).
13. F. Kramer, W. Peti, C. Griesinger, and S. J. Glaser, Optimized homonuclear Carr–Purcell- type dipolar mixing sequences, *J. Magn. Reson.* **149,** 58–66 (2001).
14. A. J. Shaka, C. J. Lee, and A. Pines, Iterative schemes for bilinear operators: Application to spin decoupling, *J. Magn. Reson.* **77,** 274–293 (1988).
15. M. H. Levitt, R. Freeman, and T. Frenkiel, Broadband heteronuclear decoupling, *J. Magn. Reson.* **47,** 328–330 (1982).
16. G. M. Clore, A. M. Gronenborn, and A. Bax, A robust method for determining the magnitude of the fully asymmetric alignment tensor of oriented macromolecules in the absence of structural information, *J. Magn. Reson.* **133,** 216–221 (1998).
17. M. Cai, H. Wang, E. T. Olejniczak, R. P. Meadows, A. H. Guanasekera, N. Xu, and S. W. Fesik, Accurate measurement of H^N–H^α residual dipolar couplings in proteins, *J. Magn. Reson.* **139,** 451–453 (1999).
18. B. Luy and S. J. Glaser, Superposition of scalar and residual dipolar couplings: Analytical transfer functions for three spins 1/2 under cylindrical mixing conditions, *J. Magn. Reson.* **148,** 169–181 (2001).
19. R. R. Ernst, G. Bodenhausen, and A. Wokaun, "Principles of Nuclear Magnetic Resonance in One and Two Dimensions," Oxford Univ. Press, New York (1987).
20. S. J. Glaser and G. P. Drobny, Assessment and optimization of pulse sequences for homonuclear isotropic mixing, *in* "Advances in Magnetic and Optical Resonance" (W. S. Warren, Ed.), Vol. 14, pp. 35–58, Academic Press, San Diego (1990).
21. U. Haeberlen, "Advances in Magnetic Resonance" (J. S. Waugh, Ed.), Supplement 1, Academic Press, New York (1976).
22. C. Griesinger, G. Otting, K. Wüthrich, and R. R. Ernst, Clean TOCSY for ^{1}H spin system identification in macromolecules, *J. Am. Chem. Soc.* **110,** 7870–7872 (1988).
23. D. M. Taylor and A. Ramamoorthy, Analysis of dipolar-coupling-mediated coherence transfer in a homonuclear two spin-1/2 solid-state system, *J. Magn. Reson.* **141,** 18–28 (1999).
24. S. J. Glaser, Coupling topology dependence of polarization-transfer efficiency in TOCSY and TACSY experiments, *J. Magn. Reson. A* **104,** 283–301 (1993).
25. D. P. Burum and R. R. Ernst, Net polarization transfer via J-ordered state for signal enhancement of low-sensitivity nuclei, *J. Magn. Reson.* **39,** 163–168 (1980).
26. E. Brunner, J. Ogle, M. Wenzler, and H. R. Kalbitzer, Molecular alignment of proteins in bicellar solutions: Quantitative evaluation of effects induced in 2D COSY spectra, *Biochem. Biophys. Res. Commun.* **272,** 694–698 (2000).
27. T. Carlomagno, T. Prasch, and S. J. Glaser, COIN TACSY, a novel approach to tailored correlation spectroscopy, *J. Magn. Reson.* **149,** 52–57 (2001).